NASA TECHNICAL NOTE

NASA TN D-2816

NASA TN D-2816

ANALYSIS OF LINEAR-INDUCTION OR TRAVELING-WAVE ELECTROMAGNETIC PUMP OF ANNULAR DESIGN

by Richard E. Schwirian

Lewis Research Center

Cleveland, Ohio

NATIONAL AERONAUTICS AND SPACE ADMINISTRATION • WASHINGTON, D. C. • MAY 1965

NASA TN D-2816

ANALYSIS OF LINEAR-INDUCTION OR TRAVELING-WAVE ELECTROMAGNETIC PUMP OF ANNULAR DESIGN

By Richard E. Schwirian

Lewis Research Center
Cleveland, Ohio

NATIONAL AERONAUTICS AND SPACE ADMINISTRATION

For sale by the Clearinghouse for Federal Scientific and Technical Information
Springfield, Virginia 22151 – Price $2.00

ANALYSIS OF LINEAR-INDUCTION OR TRAVELING-WAVE ELECTROMAGNETIC PUMP OF ANNULAR DESIGN

by Richard E. Schwirian

Lewis Research Center

SUMMARY

An analysis of a linear traveling-wave pump in which induced electrical currents flow circumferentially in a circular annulus is presented. The method of analysis is the solution of Maxwell's equations, in the form of the "magnetic" equation, in cylindrical coordinates for the axial and radial components of the magnetic flux density. Effects of fluid and duct-wall conductivity on the distribution and magnitude of the magnetic field are included as well as two-dimensional effects. General solutions are specialized to specific configurations and conditions by applying the appropriate magnetic boundary conditions at each fluid-duct-wall, duct-wall-core, and core-space interface. The excitation currents in the coils are approximated by an equivalent surface current density at the interface between the outer core and the duct wall in order to be consistent with the method of analysis.

The concept of multiple passages in a single pumping unit as compared with multiple pumps for use in parallel radiator coolant loops is proposed and discussed. Approximate performance corrections are presented. The analysis, with the performance corrections for multiple-passage pumps, is then used to design three lithium radiator coolant pumps, each with an output pressure of 30 pounds per square inch. Each pump represents a different means for attaining the same objective, namely, the pumping of lithium at 1200° F with a total system flow rate of 40 pounds per second.

For the particular design conditions assumed, an optimization procedure based on maximizing efficiency for a fixed peak coil current density over the full range of slip and a range of fluid velocities and pump radial dimensions is outlined.

A single-passage 40-pound-per-second pump was designed at an efficiency of 21.9 percent with a weight of 145 pounds. A multiple-passage pump of the same capacity was designed that had an efficiency of 20.7 percent and weighed 149 pounds. Finally, a single-passage pump was designed that possessed an efficiency of 16.4 percent and weighed 68 pounds (total weight of four pumps, 272 lb). Each of these pumps, for a design pressure of 30 pounds per square inch, is a reasonable magnetic-hydraulic design for a space power system.

INTRODUCTION

In space electric powerplant systems that would use the liquid alkali metals as the working fluid and/or as a heat-transfer medium, a need exists for pumping units of high reliability, low weight, and high efficiency. To date, attention has been focused primarily on the canned-motor pump for space applications because of its somewhat higher predicted efficiency and lower weight as compared with conventional electromagnetic pumps. Nevertheless, bearing, seal, and cavitation damage problems associated with impeller pumps in liquid-metal systems suggests that a certain weight penalty might be acceptable in order to take advantage of the higher reliability potentially available with electromagnetic pumps. It can be argued that the electromagnetic pump is inherently more reliable because of its simplicity and the complete absence of seals or other moving parts. Furthermore, better pumping characteristics under cavitating flow conditions should be obtainable in the electromagnetic pump because the pumping force is a body force and extreme pressure gradients within the pump are avoided. Recent pump design studies (refs. 1 to 3) indicate that even though electromagnetic pumps that have been built to date are quite heavy, it is possible in designing for space power applications to reduce the weight of electromagnetic pumps by a factor of about 10. This weight reduction is accomplished largely by decreasing the weight of the pump structural frame and, to a lesser degree, by eliminating unnecessary magnetic material and utilizing magnetic materials with higher saturation flux densities.

For space power systems, the induction electromagnetic pump, because it lacks electrodes, is inherently more reliable than the conduction electromagnetic pump. The annular linear induction pump, furthermore, has several advantages over its flat counterpart because it has greater structural integrity, is more adaptable to normal piping systems, and allows greater design freedom in the coil configuration. The annular design also has a basically greater output capability since the path followed by the induced currents has a lower resistance than the path followed in a corresponding flat pump. An annular pump was proposed in about 1927 by Einstein and Szilard (ref. 4). Since then, a number of analyses has been performed, but generally they assume one dimensionality of the magnetic field or are two-dimensional descriptions that lack completeness.

Okhremenko (ref. 5) performed an analysis on a flat linear induction pump but assumed nonconducting duct walls. In his analysis, the magnetic equations in rectangular coordinates were solved, and a suitable method for considering the effect of finite pump width was included. Few results were given, so that comparisons with the results obtained in the present analysis are difficult.

The decrease in magnetic-field intensity due to current flow in the fluid and duct is sometimes accounted for by introducing a "load current" (refs. 1 to 3) that must be

added to the "magnetizing current" in the coils to compensate for fluid and duct-wall current flow. Such approximations generally assume the magnetic field to be constant across the duct and thus neglect the distortion of the magnetic field at high values of slip.

This report presents a more comprehensive theoretical treatment of the annular traveling-wave pump, so that optimum design configurations can be evolved and more accurate predictions of performance of these designs can be obtained. The appropriate equations resulting from this treatment were programed on an IBM 7090 computer and then used to calculate the performance of several pumping configurations for use in a radiator coolant loop. The particular application considered is lithium at 1200° F contained in a columbium - 1-percent-zirconium duct for a pressure rise of 30 pounds per square inch and a total system flow rate of 40 pounds per second. Performance characteristics of several pumping configurations for producing this pressure and flow are investigated and compared. The configurations investigated are (1) one single-passage pump with a flow rate of 40 pounds per second for a single-loop system, (2) one quadruple-passage pump with a total flow rate of 40 pounds per second for a four-loop system, and (3) four single-passage pumps, each with a flow rate of 10 pounds per second for a four-loop system.

ANALYSIS

Equations and Assumptions

The system to be analyzed is shown in figure 1. A conducting fluid flows in the annulus between inner and outer cores of a high-permeability magnetic material. A traveling magnetic wave produced by polyphase coils moves with velocity $\vec{v}_w$ through the conducting fluid, which moves with velocity $\vec{v}_f$. The analysis is restricted to the central portion of the pump, end effects being neglected, so that the wave can be assumed to vary periodically as a function of time and the axial coordinate z. The method of analysis is to solve the magnetic field equations in cylindrical coordinates and to apply the appropriate boundary conditions on the radial and axial components of the magnetic field at each fluid - duct-wall, duct - wall-core, and core-space interface. In this way the effect of duct-wall conductivity, as well as fluid conductivity, on the distribution and magnitude of the magnetic field throughout the pump is automatically included. As opposed to other analyses (refs. 1 to 3) that assume a purely transverse field, results are not restricted to low values of the gap-to-wavelength ratio. Nontransverse field effects also become important, even for low values of gap-to-wavelength ratio g_m/λ (fig. 2), if either the fluid or the duct wall has a fairly high electrical conductivity and if moderate- to high-slip performance is desired. In this report, situations in which all these

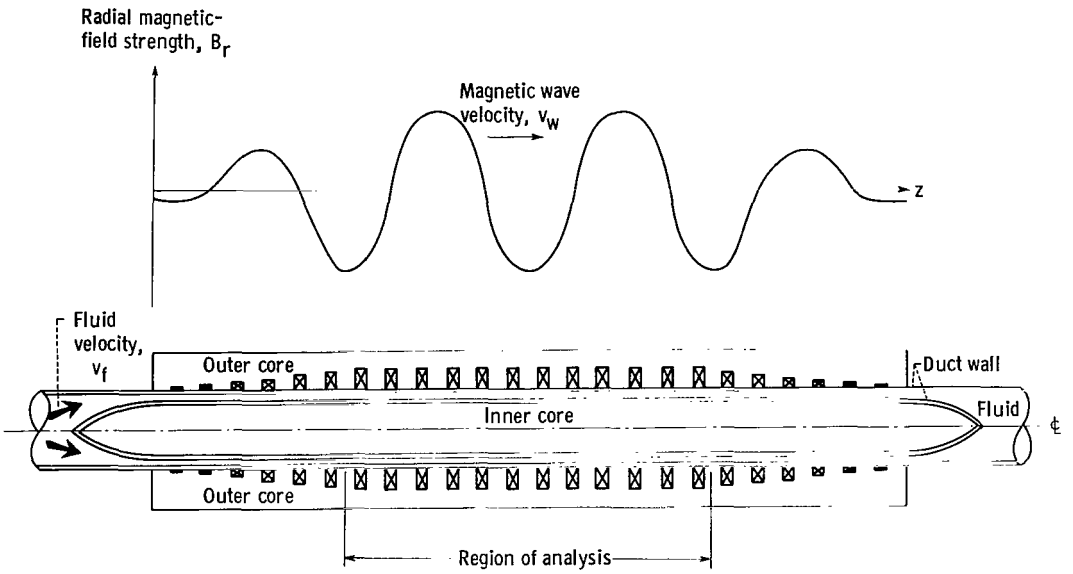

Figure 1. - Annular traveling-wave pump.

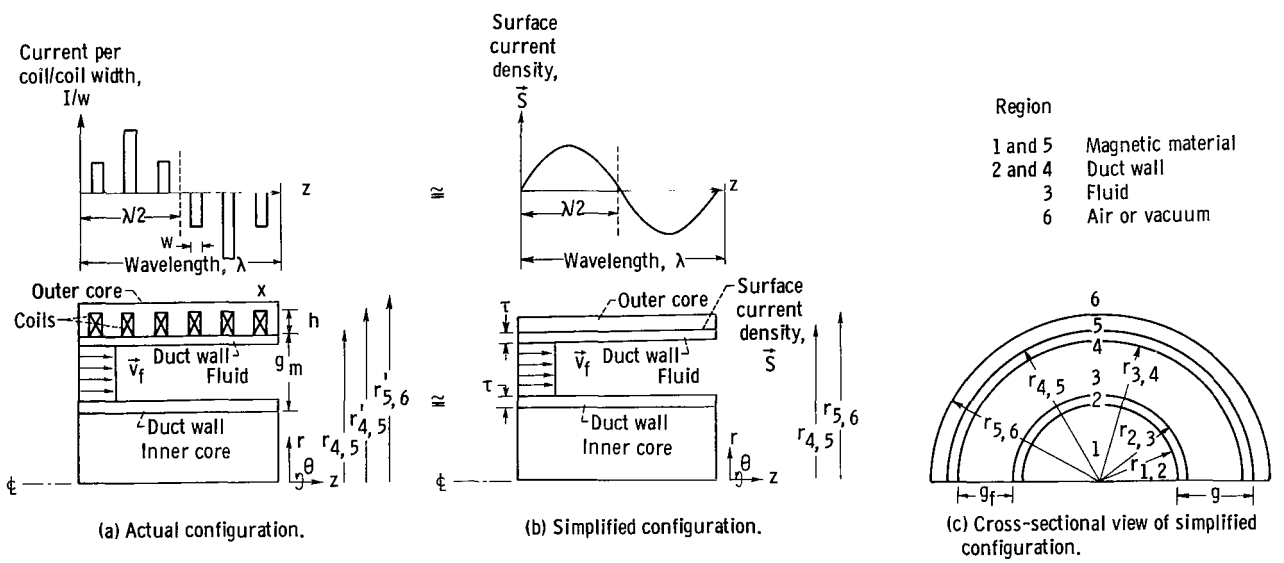

Figure 2. - Surface current approximation and idealized pump configuration.

effects can be important are investigated.

The assumptions made are

(1) End effects at the duct inlet and outlet can be neglected.

(2) The fluid velocity is constant throughout the duct.

(3) Current flow in the coils can be approximated by the flow of an ideal surface current between the duct wall and the outer core (fig. 2).

(4) The effect of nonzero coil height on the magnetic field in the gap is negligible.

With regard to the second assumption, some work has been done by Turcotte and Lyons (ref. 6) in estimating the Hartmann effect in traveling-wave devices. Hartmann flow, which is a channel flow of a viscous, electrically conducting fluid in a steady magnetic field (ref. 7), has the undesirable effect of producing a larger friction factor than those produced by ordinary laminar or turbulent flow. However, Murgatroyd (ref. 8) has shown experimentally that Hartmann flow (ref. 7) is not a proper description, except at high values of the ratio of Hartmann number ($|\vec{B}| g_f \sqrt{\frac{\sigma_3}{\mu_f}}$) to Reynolds number, if the flow at zero magnetic-field strength is turbulent. (Symbols are defined in the appendix.) Because of the complexities involved in using the work of Turcotte and Lyons (ref. 6) and the question of applicability to the assumed configuration, head-loss calculations in the present analysis are based on simple turbulent flow formulas (ref. 9).

The third and fourth assumptions were made in order to conform with the method of analysis and still preserve a well-defined gap. The coil height is assumed to be zero, and the surface current magnitude is assumed to vary sinusoidally with time and the axial coordinate z (fig. 1).

With these assumptions the problem is essentially reduced to one of obtaining expressions for the magnetic-field strength $\vec{B}$ and the current density $\vec{j}$ so that computations of output power and electrical losses can be obtained. In this analysis the mks system is used for simplicity of presentation, although results are presented primarily in the English system. To perform the analysis, Maxwell's equations and Ohm's law for an isotropic, charge-free medium are required. These are, with displacement current terms neglected,

$$\text{curl } \vec{E} = -\frac{\partial \vec{B}}{\partial t} \tag{1}$$

$$\text{curl } \vec{B} = \mu \vec{j} \tag{2}$$

$$\text{div } \vec{B} = 0 \tag{3}$$

$$\text{div } \vec{E} = 0 \tag{4}$$

$$\vec{j} = \sigma\left[\vec{E} + \vec{v} \times \vec{B}\right] \tag{5}$$

These equations can be reduced to the "magnetic" equation

$$\nabla^2 \vec{B} = \mu\sigma \frac{\partial \vec{B}}{\partial t} - \mu\sigma \text{ curl}(\vec{v} \times \vec{B}) \tag{6}$$

the solutions of which are subject to the condition

$$\operatorname{div} \vec{B} = 0 \tag{3}$$

For the system under consideration $\vec{v}$ is assumed to be a known constant. Equations (6) and (3) can then be solved for the magnetic-field strength $\vec{B}$ and then used to compute the current density $\vec{j}$ from equation (2).

General Solution of Equations

For the configuration described by figure 2 it is clear that an axisymmetric solution is desired. Hence,

$$\frac{\partial}{\partial \theta} = 0$$

Since the applied magnetic field consists of a traveling wave propagating to the right as in figure 1, it is logical to assume solutions for $\vec{B}$ of the form

$$\vec{B}(r, z, t) = e^{-i\omega t} \sum_{\substack{m=-\infty \\ m \neq 0}}^{\infty} \vec{R}^{(m)}(r) e^{imkz} \tag{7}$$

In equation (7) it is assumed that the time dependence of $\vec{B}$ on t is purely sinusoidal; whereas, the dependence of $\vec{B}$ on z is merely periodic with period λ. Therefore, $\vec{R}^{m}(r)$ can be written

$$\vec{R}^{(m)}(r) = \alpha^{(m)}(r)\hat{r} + \beta^{(m)}(r)\hat{z} \tag{8}$$

Since the electrical currents in the exciting coils flow in circumferential paths and the induced electrical currents also flow in circumferential paths, $\vec{R}^{m}(r)$ has no component in the θ-direction. Substituting equations (7) and (8) into equation (6) and equating coefficients of e^{imkz} result in the following equations:

$$\frac{1}{r}\frac{d}{dr}\left[r\frac{d\alpha^{(m)}}{dr}\right] + \left\{\left[\gamma^{(m)}\right]^2 - \frac{1}{r^2}\right\}\alpha^{(m)} = 0 \tag{9}$$

$$\frac{1}{r}\frac{d}{dr}\left[r\frac{d\beta^{(m)}}{dr}\right]+\left\{\left[\gamma^{(m)}\right]^2\right\}\beta^{(m)}=0 \tag{10}$$

where

$$\gamma^{(m)}=\sqrt{i\left(\frac{2\pi m\mu\sigma}{\lambda}\right)v_s^{(m)}-m^2k^2} \tag{11}$$

and

$$v_s^{(m)}=\frac{\lambda\omega}{2\pi m}-v \tag{12}$$

Equation (10) was obtained with the help of equation (3), which can be written

$$\frac{\partial B_z}{\partial z}=-\frac{1}{r}\frac{\partial}{\partial r}rB_r$$

The quantity $v_s^{(m)}$ is the velocity of the mth component of $\vec{B}$ relative to the moving medium. The general solutions of equations (9) and (10) are

$$\alpha^{(m)}(r)=a_1^{(m)}J_1\left[\gamma^{(m)}r\right]+a_2^{(m)}Y_1\left[\gamma^{(m)}r\right] \tag{13}$$

$$\beta^{(m)}(r)=b_1^{(m)}J_0\left[\gamma^{(m)}r\right]+b_2^{(m)}Y_0\left[\gamma^{(m)}r\right] \tag{14}$$

where the symbols J and Y denote Bessel functions of the first and second kind, respectively. Equation (3) relates $a_1^{(m)}$ to $b_1^{(m)}$ and $a_2^{(m)}$ to $b_2^{(m)}$ as follows:

$$b_1^{(m)}=\frac{i\gamma^{(m)}a_1^{(m)}}{mk} \tag{15}$$

$$b_2^{(m)}=\frac{i\gamma^{(m)}a_2^{(m)}}{mk} \tag{16}$$

Equation (14) can now be written

$$\beta^{(m)}(r)=\frac{i\gamma^{(m)}}{mk}\left\{a_1^{(m)}J_0\left[\gamma^{(m)}r\right]+a_2^{(m)}Y_0\left[\gamma^{(m)}r\right]\right\} \tag{17}$$

Boundary Conditions

In order to provide a tractable boundary condition at the interface between the outer core and the outer duct wall, it is assumed, for purposes of analysis, that the coils can be replaced by a continuous surface current at this location. The simplified configuration is depicted in figure 2 (p. 4) and compared to the actual configuration. The actual coil currents are step functions of the axial coordinate; whereas, the surface current varies sinusoidally in the axial direction. The various regions are explained and assigned one of the numbers 1 to 6 for convenience in analysis. An interface between two regions is designated by the radial location of that interface. For instance, the interface between regions 1 and 2 will be designated by $r_{1,2}$.

At the interface between two isotropic media G and H, $\vec{B}$ must satisfy

$$\hat{n} \cdot (\vec{B}_G - \vec{B}_H) = 0 \tag{18}$$

$$\hat{n} \times \left(\frac{\vec{B}_G}{\mu_G} - \frac{\vec{B}_H}{\mu_H} \right) = \vec{S}_{G,H} \tag{19}$$

where $\hat{n}$ is a unit vector normal to the interface and $\vec{S}_{G,H}$ is the surface current density between the two media. For the system under consideration, equation (18) is a condition on B_r and equation (19) is a condition on B_z. Equations (18) and (19) can be written

$$B_{r,\ell}(r_{\ell,\ell+1}) = B_{r,(\ell+1)}(r_{\ell,\ell+1}) \tag{20}$$

$$\frac{B_{z,\ell}(r_{\ell,\ell+1})}{\mu_\ell} - \frac{B_{z,(\ell+1)}(r_{\ell,\ell+1})}{\mu_{\ell+1}} = S_{\ell,\ell+1} \tag{21}$$

where $B_{r,\ell}(r_{\ell,\ell+1})$ and $B_{z,\ell}(r_{\ell,\ell+1})$ are the radial and axial components of the magnetic field at the interface between medium ℓ and $\ell + 1$, μ_ℓ and $\mu_{\ell+1}$ are the permeabilities of media ℓ and $\ell + 1$, and $S_{\ell,\ell+1}$ is the surface current density between mediums ℓ and $\ell + 1$.

Equations (20) and (21), when values of ℓ from 1 to 5 are substituted, yield 10 equations in 12 unknowns for each value of the index m. To reduce the number of unknowns for each index m by 2, it is sufficient to recall that $\vec{B}$ must be finite everywhere. Because of the nature of the functions J_1, Y_1, J_0, and Y_0 the implication is that

$$a_{2,1}^{(m)} = a_{1,6}^{(m)} = 0 \tag{22}$$

In equation (22) the constants $a_{1,6}^{(m)}$ and $a_{2,1}^{(m)}$ are defined by equation (13); the second subscript refers to the medium. If $a_{2,1}^{(m)}$ were not zero, $\vec{B}$ at $r = 0$ would be infinite. If $a_{1,6}^{(m)}$ were not zero, $\vec{B}$ would approach infinity as r approached infinity since $\gamma^{(m)}$ is a complex number.

The set of equations (20) and (21) now constitutes a completely solvable set, and by using equations (13) and (17) the 10 remaining unknown constants $a_{1,\ell}^{(m)}$ and $a_{2,\ell}^{(m)}$ for $\ell = 1$ to 6 can be determined if $\vec{S}_{\ell,\ell+1}$ is assumed to be of the form

$$\vec{S}_{\ell,\ell+1} = e^{-i\omega t} \sum_{\substack{m=-\infty \\ m\neq 0}}^{\infty} S_{\ell,\ell+1}^{(m)} e^{imkz} \hat{\theta} \tag{23}$$

For practical purposes $\vec{S}_{\ell,\ell+1} = 0$ except for $\ell = 4$; therefore, equation (23) can be rewritten

$$\vec{S}_{\ell,\ell+1} = \delta_{\ell,4} e^{-i\omega t} \sum_{\substack{m=-\infty \\ m\neq 0}}^{\infty} S_{\ell,\ell+1}^{(m)} e^{imkz} \hat{\theta} \tag{24}$$

It is apparent that by Fourier analysis the expansion coefficients $S_{\ell,\ell+1}^{(m)}$ can be selected so that the function

$$\delta_{\ell,4} \sum_{\substack{m=-\infty \\ m\neq 0}}^{\infty} S_{\ell,\ell+1}^{(m)} e^{imkz}$$

represents any practical given coil configuration. If equations (17) and (21) are used, the coefficients $a_1^{(m)}$ and $a_2^{(m)}$ can be related to the expansion coefficients $S_{\ell,\ell+1}^{(m)}$.

The magnitude of the problem outlined is greatly reduced if the magnetic field $\vec{B}$ and the surface current $\vec{S}_{\ell,\ell+1}$ can be assumed to vary not only periodically but sinusoidally with z. In this case equation (24) reduces to

$$\vec{S} = \delta_{\ell,4} S_{\ell,\ell+1}^{(1)} e^{i(kz-\omega t)} \hat{\theta}$$

$$= \delta_{\ell,4} S e^{i(kz-\omega t)} \hat{\theta} \tag{25}$$

The subscript $\ell, \ell+1$ is dropped because it is assumed that $\vec{S}$ is nonzero only between regions 4 and 5. Also $S^{(1)}$ is replaced by S because only the first harmonic is being considered.

For the purpose of this analysis, equation (25) will be assumed sufficient to describe the analytical problem. The coefficient S, furthermore, will not be obtained by Fourier analysis but will be approximated by a simpler technique to be discussed in the next section.

Surface Current Approximation

The surface current approximation is used to relate the magnetic field directly to the coil currents without assuming uniformity of the field across the gap and at the same time to retain a well-defined gap $r_{4,5} - r_{1,2}$ (fig. 2). Inherent in this approximation are the assumptions that, with regard to the shaping and magnitude of the field in the gap, (1) the radial height of the coils has little effect and (2) the axial spacing and the discrete nature of the coil currents as functions of z have little effect.

The first of these assumptions should be fairly valid if the permeability of the cores (regions 1 and 5, fig. 2) is sufficiently greater than the permeability of the gap (regions 2 to 4, fig. 2) and if the cross-sectional area between $r_{4,5}$ and $r_{5,6}$ (fig. 2) in the simplified pump is preserved as the cross-sectional area between $r'_{4,5}$ and $r'_{5,6}$ in the real pump.

The second assumption concerning the z-spacing of the coils is a more serious one. If the coil width w is small (fig. 3(a)) compared with the core width between coils x, approximating the coil currents by a continuous function of z may not be legitimate. However, if x is small compared with w (fig. 3(b)), it is questionable whether a well-defined gap exists. The lack of definition of the air gap results from the increase in the reluctance of the radial flux path between coils as x decreases. It is possible that this reluctance could become so high that secondary magnetic flux would flow directly from the top of the coils to the inner core by way of a path that includes the coils. If this happens, the gap is no longer given simply by $g_m = r_{4,5} - r_{1,2}$ since some secondary flux flows through the larger gap $(r_{4,5} + h) - r_{1,2}$. Also, the flux density in that portion of the magnet between coils will be higher than the flux density elsewhere, and saturation might occur there even for low excitation currents.

As a result of these restrictions, the analysis should be limited to pumps for which the assumption of sinusoidal variation of $\vec{S}$ with z is legitimate, such as the case where a large number of phases is present. The coil height h should also be small. In order to use the results of the analysis presented previously, it is assumed that 3 is a large number of phases. The surface current $\vec{S}$ and coil electrical losses will be determined by assuming three phases.

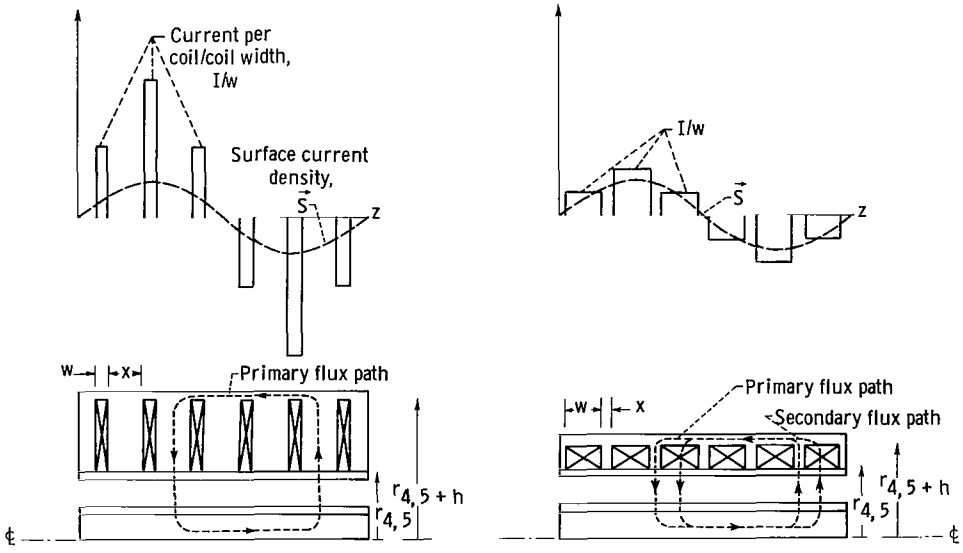

(a) Small coil width. Total flux in gap approximates primary flux.

(b) Large coil width. Total flux in gap equals primary plus secondary flux.

Figure 3. - Effect of coil width on validity of surface current approximation and choice of gap height.

Since, in practice, the magnetic field will be produced by coils of finite extent in the z-direction rather than by a continuous surface current, it is necessary to relate the magnitude of the current in the coils to the magnitude of the equivalent surface current. The surface current $\vec{S}$ is given by the equation

$$\vec{S} = \delta_{\ell,4} S e^{i(kz-\omega t)} \hat{\theta} \tag{26}$$

The actual excitation currents are given by

$$\vec{I} = I e^{-i\omega t} e^{i\Phi} \hat{\theta} \tag{27}$$

where $e^{i\Phi}$ represents a phase factor that depends on the location of a particular coil. Since S is the peak value of $\vec{S}$ and there are six coils per wavelength, a sufficient approximation of S is

$$S = \frac{I}{\lambda/6} = \frac{6I}{\lambda} \tag{28}$$

Computation of Output Power and Losses

The constants $a_{1,\ell}$ and $a_{2,\ell}$ for ℓ = 1 to 6 having been determined by solving the set of equations (20) and (21), the magnetic-field strength $\vec{B}$ and the current density $\vec{j}$

can be computed everywhere. Since only $B_{r,\ell}$ and $B_{z,\ell}$ exist and $\partial/\partial\theta = 0$, $\vec{j}_\ell$ has a component in the θ-direction only,

$$\vec{j}_\ell = \frac{\text{curl } \vec{B}_\ell}{\mu_\ell} = \frac{1}{\mu_\ell}\left(\frac{\partial B_{r,\ell}}{\partial z} - \frac{\partial B_{z,\ell}}{\partial r}\right)\hat{\theta}$$

Using equations (7), (8), (13), and (17) only for the $m = 1$ component yields

$$\frac{\partial B_{r,\ell}}{\partial z} = ikB_{r,\ell}$$

and

$$-\frac{\partial B_{z,\ell}}{\partial r} = \frac{i\gamma_\ell^2 B_{r,\ell}}{k}$$

but

$$\frac{i\gamma_\ell^2}{k} = \mu_\ell \sigma_\ell v_{s,\ell} - ik$$

so that

$$\vec{j}_\ell = j_\ell\hat{\theta} = -\sigma_\ell v_{s,\ell} B_{r,\ell}\hat{\theta}$$

$$j_\ell = -\sigma_\ell v_{s,\ell} B_{r,\ell} \tag{29}$$

If only real excitation currents are assumed (only the real part of eq. (26) is taken), performance calculations must be based on real magnetic fields and real induced currents. In such a case the magnetic output power per wavelength is

$$W_\lambda = 2\pi \int_0^\lambda \int_{r_{2,3}}^{r_{3,4}} \left[\Re(\vec{j}_3) \times \Re(\vec{B}_3)\right] \cdot \vec{v}_f r \, dr \, dz \tag{30}$$

where $\Re$ implies real.

The pressure increase over one wavelength due to magnetic forces can be computed from equation (30) since fluid velocity $\vec{v}_f$ is a constant and can be factored from the equation

$$\Delta p_\lambda = \frac{W_\lambda}{|\vec{v}_f| A_f} \tag{31}$$

for $A_f = \pi\left(r_{3,4}^2 - r_{2,3}^2\right)$. The electrical losses in the fluid, duct, and magnet are combined in $W_{J\lambda}$ where

$$W_{J\lambda} = \sum_{\ell=1}^{5} W_{J\lambda,\ell} = 2\pi \sum_{\ell=1}^{5} \frac{1}{\sigma_\ell} \int_0^\lambda \int_{r_{\ell-1,\ell}}^{r_{\ell,\ell+1}} \left[\Re(\vec{j}_\ell) \cdot \Re(\vec{j}_\ell)\right] r \, dr \, dz \tag{32}$$

(This sum omits region 6 since this region represents either air or vacuum where $\vec{j} = 0.$)

The electrical losses for six coils per wavelength are

$$W_{c\lambda} = 3I^2R \cong \frac{3j_c^2}{\sigma_c} \pi\left[(r_{4,5} + h)^2 - r_{4,5}^2\right] w \tag{33}$$

Hydraulic losses, if turbulent flow is assumed, can be computed from the equation (ref. 9)

$$W_{V\lambda} = \left(\frac{C_f \rho_f v_f^2}{8}\right)\left[2\pi\lambda(r_{3,4} + r_{2,3})\right] v_f$$

$$= (\text{Fluid-to-duct shear stress})(\text{Duct area})(\text{Fluid velocity}) \tag{34}$$

The friction coefficient C_f used is defined by the formulas (ref. 9)

$$C_f = \frac{0.3164}{Re^{0.25}} \quad \text{for} \quad 2000 < Re < 10^5 \tag{35}$$

and

$$C_f = 0.0032 + \frac{0.221}{Re^{0.237}} \quad \text{for} \quad Re > 10^5 \tag{36}$$

where

$$Re = \frac{2\rho_f v_f (r_{3,4} - r_{2,3})}{\mu_f}$$

The pressure drop due to viscous forces can be computed in a similar manner:

$$\Delta p_{V\lambda} = \frac{\left(C_f \rho_f v_f^2/8\right)\left[2\pi(r_{3,4} + r_{2,3})\right]}{A_f}\,\lambda \tag{37}$$

The net pressure rise per wavelength is then

$$\Delta p_{n\lambda} = \Delta p_{\lambda} - \Delta p_{V\lambda} \tag{38}$$

Performance Parameters

The parameters of most interest in evaluating a pump for a space power system are its overall efficiency η, its head-flow characteristics, and its weight-power ratio or specific weight w_{sp}. Efficiency η and weight-power ratio w_{sp} are, ideally, defined as

$$\eta_{id} = \frac{W_{n\lambda} 100}{W_{T\lambda}} \tag{39}$$

where

$$W_{n\lambda} = W_{\lambda} - W_{V\lambda}$$

$$W_{T\lambda} = W_{\lambda} + W_{c\lambda} + W_{J\lambda}$$

and

$$w_{sp,\,id} = (\text{Weight of pump per wavelength})/W_{n\lambda} \tag{40}$$

The pump weight per wavelength consists of the sum of the inner and outer core, the duct wall, and the coil weight per wavelength. In practice the weight-power ratio is larger than the ideal $w_{sp,\,id}$ suggested herein because the coil height is not zero and also because of the grading of the coil windings at the ends of the pump; the result is a lower output for these sections. Letting the cross-sectional area between $r_{4,5}$ and $r_{5,6}$ in the ideal case equal the cross-sectional area between $r'_{4,5}$ and $r'_{5,6}$ in the actual case and assuming a coil height h result in an increase in pump weight per wavelength because of the former effect of approximately

$$\begin{aligned}\Delta M_{\lambda} &\cong \pi\left[(r_{4,5} + h)^2 - r_{4,5}^2\right]\left[6w\rho_c + (\lambda - 6w)\rho_m\right] \\ &= \pi h(h + 2r_{4,5})\left[6w\rho_c + (\lambda - 6w)\rho_m\right]\end{aligned} \tag{41}$$

Since the method of grading the windings at the ends of the pump is somewhat arbitrary, it will be assumed that, whatever method is employed, the effect is to decrease the output power over the end sections by one-half of that in the main portion of the pump. If the end sections consist of one wavelength apiece and the number of wavelengths in the pump, including the end sections, is d, the ideal weight-power ratio must be multiplied by a factor of $d/(d - 1)$.

The combined effects of nonzero coil height and grading of the coils in the pump end sections result in an actual w_{sp} of

$$w_{sp} = \frac{d}{d - 1}\left(w_{sp,\,id} + \frac{\Delta M_\lambda}{w_{n\lambda}}\right) \tag{42}$$

Similarly, a factor of $100\left[W_{V\lambda}/(d - 1)W_{T\lambda}\right]$ must be subtracted from η_{id} to correct for added hydraulic losses in the end sections:

$$\eta = \eta_{id} - 100\left[\frac{W_{V\lambda}}{(d - 1)W_{T\lambda}}\right] \tag{43}$$

A parameter of particular interest in an electromagnetic pump is the maximum magnetic flux density in the inner and outer cores due to saturation flux density considerations. The analysis outlined in the preceding sections provides a means for calculating $|\vec{B}|_{id}$ for the case where $|\vec{B}|_{id}$ is produced by a surface current at $r = r_{4,5}$ that varies in a purely sinusoidal manner with z-position and time. In this report a maximum value of $|\vec{B}|_{id}$ is obtained that is based on calculations of 80 points in the range $0 \leq z \leq \lambda$ and $0 \leq r \leq r_{1,2}$ where $r_{4,5} \leq r \leq r_{5,6}$. A corrected maximum value of $|\vec{B}|_{id}$, referred to as $|\vec{B}|_m$, is then given. The correction is necessary because, in a real pump, a nonzero volume is occupied by the exciting coils in region 5, which results in less available magnetic material between the coils than that available for the ideal configuration. The flux density is, therefore, somewhat higher in this region than the ideal analysis indicates. A suitable estimate of the increase in flux density is obtained by assuming that the actual flux density is greater than the ideal value by a factor of $\lambda/(\lambda - 6w)$ (ratio of ideal available magnetic material between coils to actual available magnetic material between coils):

$$|\vec{B}|_m = \frac{\lambda}{\lambda - 6w}|\vec{B}|_{m,\,id} \tag{44}$$

In region 1, $|\vec{B}|_m \cong |\vec{B}|_{m,\,id}$ since there are no coils there. Although the corrections for real pump effects outlined herein are not rigorous, they form the basis for the practical calculation of predicted performance of actual pumps.

APPLICATION OF ANALYSIS

The equations presented in the previous section were programed on an IBM 7090 computer to obtain theoretical performance calculations of specific pump designs. Pump requirements were established to be typical of a radiator coolant pump in an advanced alkali metal space power system with an electrical output of approximately 1 megawatt. The resulting pump specifications were

Fluid	Lithium
Fluid temperature, ^{o}F	1200
Total flow, lb/sec	40
Developed pressure, lb/sq in.	30

The significant properties of lithium at 1200^{o} F are

Electric conductivity, $(ohm\text{-}m)^{-1}$	2.56×10^{6}
Density, lb/cu ft	29.3
Absolute viscosity, $(lb)(sec)^{2}/ft$	2×10^{-4}
Vapor pressure, lb/sq in. abs.	3×10^{-3}

The primary requirement for this application is extremely high reliability; good unattended performance must be maintained for 1 year or more. Also, for space applications weight should be minimized and reasonable efficiency maintained in order to lessen the overall weight penalty to the system.

The particular designs considered were assumed to operate without any cooling of the coils and the magnet except by the working fluid. Such operation is feasible if the coils are electrically insulated with a ceramic oxide such as alumina and the magnet is made of high-cobalt iron. The duct material was assumed to be columbium - 1 percent zirconium with a thickness of 0.03 inch. Copper at 1200^{o} F was taken to be coil material and was assumed to carry a peak current density j_c of 12 000 amperes per square inch. For all calculations the wavelength was held at 6 inches, and the number of wavelengths was held at 4.

Multiple-Passage Concept

Generally speaking the efficiency and weight-power ratio of electromagnetic pumps are, respectively, increasing and decreasing functions of output power. An electromagnetic pump is, therefore, most desirable for systems requiring high flows and large

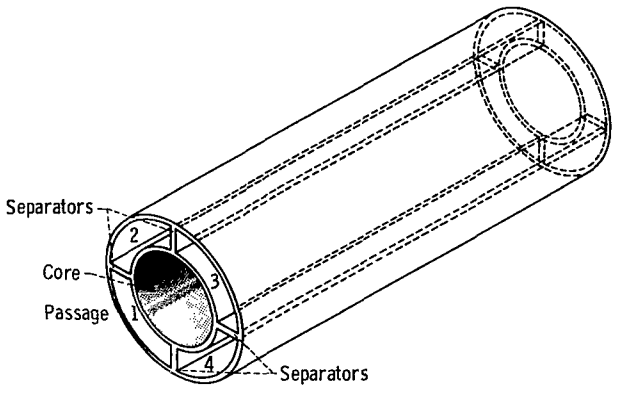

Figure 4. - Multiple-passage concept.

developed pressures. In the coolant radiator of a space power system, however, the possibility of meteoroid penetration leads to a requirement for a certain amount of redundancy, particularly in a radiator coolant loop. This implies the need for a large number of pumps of low output power. Since the meteoroid hazard is most serious for the radiator, a single pump of fairly large output power could fulfill the entire pumping requirement if it could serve as a pump for all of the parallel systems without allowing the fluids in each system to mix. An electromagnetic induction pump should be capable of this type of performance if the flow region is divided into multiple passages with separators of the same material as the duct wall (fig. 4). If there is only a small number of passages and the separators are thin and reasonably conductive, performance should differ only slightly from that of a pump of equal dimensions with no separators. If the number of passages is large, however, hydraulic losses could seriously degrade the performance. Low performance would also be expected if the separators were highly resistive, which is not normally the case.

If, because of a failure, the fluid were depleted from one or more of the redundant systems for which the pump in figure 4 was supplying pumping power, the output power and efficiency of each passage would be decreased by an amount that would depend on both the number of passages depleted and their location. This decrease would occur because, although the induced electric field in the fluid would be essentially the same as in normal operation, the induced electrical currents could no longer flow through the depleted passage. Whereas current path lines normally close by way of purely circumferential paths, they would now tend to close by way of axial paths. The relative resistance of the current paths in full passages would be increased, and the reaction current and the output power of those passages would thereby be reduced. In general, the performance of any passage would be a decreasing function of the number of passages depleted. The situation would be particularly acute for passages immediately adjacent to depleted passages. The amount of performance degradation, in any case, is uncertain and requires further analysis. Such an analysis is beyond the scope of the present report.

The effect of a depleted passage on the performance of remaining passages can be reduced somewhat by making the wavelength of the pump, and therefore the resistance of the current paths, as small as possible. There is, of course, a limit to how small the wavelength can be made, depending on such quantities as allowable coil current density j_c, coil width w, etc.

Approximate Performance Corrections for Multiple-Passage Pumps

For a multiple-passage pump an exact determination of the magnetic field and the current density in the fluid and the pump is not practical; however, if the passage separators are thin and of a reasonably conductive material, their effects on the electric and magnetic fields should be negligible. It will therefore be assumed that the magnetic field and the current density throughout the pump are unchanged by the presence of passage separators in the fluid gap. Therefore, the only performance corrections necessary are an additional electrical loss due to the higher resistivity of the separators and additional hydraulic losses due to a larger wetted perimeter. If q is the number of passages, an approximate corrected value of $W_{J\lambda,3}$ (eq. (31)) is

$$(W_{J\lambda,3})_{\text{corrected}} =$$

$$\left[\frac{(\text{fluid cross-sectional area}) + \frac{\sigma_3}{\sigma_4}(\text{separator cross-sectional area})}{\pi\left(r_{3,4}^2 - r_{2,3}^2\right)}\right](W_{J\lambda,3})_{\text{uncorrected}}$$

$$= \left[1 + \frac{4q\tau}{\pi\left(r_{3,4}^2 - r_{2,3}^2\right)}\left(\frac{\sigma_3}{\sigma_4} - 1\right)\right](W_{J\lambda,3})_{\text{uncorrected}} \tag{45}$$

where $\tau = r_{3,4} - r_{2,3}$ and it is assumed that the separators are of the same material and thickness as the duct wall. Hydraulic losses for multiple passages should be based on a new wetted perimeter and fluid cross-sectional area. It will be assumed for simplicity, however, that the fluid cross-sectional area is the same as that in the single-passage case. This assumption is reasonable for a small number of passages with thin separators.

Friction factor C_f (eqs. (35) and (36)) should be based on a corrected Reynolds number:

$$(\text{Re})_{\text{corrected}} = \frac{2\rho_f v_f}{\mu_f} \frac{\pi\left(r_{3,4}^2 - r_{2,3}^2\right)}{2\pi(r_{3,4} + r_{2,3}) + 2q(r_{3,4} - r_{2,3})}$$

Similarly, hydraulic losses and pressure drop per wavelength are

$$(W_{V\lambda})_{\text{corrected}} = \left(\frac{C_f \rho_f v_f^2}{2}\right)\left[2\pi(r_{3,4} + r_{2,3}) + 2q(r_{3,4} - r_{2,3})\right]\lambda v_f \tag{46}$$

$$(\Delta p_{V\lambda})_{\text{corrected}} = \left(\frac{C_f \rho_f v_f^2}{2A_f}\right)\left[2\pi(r_{3,4} + r_{2,3}) + 2q(r_{3,4} - r_{2,3})\right]\lambda \qquad (47)$$

For the results presented in this report the additional weight resulting from the presence of passage separators is neglected in computations of pump weight and weight-power ratio.

Optimization and Performance Evaluation of Selected Designs

In a space power system redundancy of coolant loops is desirable for the reasons outlined previously. If parallel loops are utilized, the problem of supplying pumping power remains. Separate pumping units are one solution. The use of multiple passages in a central pumping unit, however, provides a lower weight, higher efficiency method for attaining this objective. It was therefore decided to investigate the performance of three types of pumps for a radiator coolant system that required pumping power at a developed pressure of 30 pounds per square inch and a total system flow rate of 40 pounds per second. Performance is calculated for no redundancy (one single-passage pump at 40 lb/sec), quadruple redundancy by means of separate passages (one quadruple-passage pump at a total flow of 40 lb/sec) and quadruple redundancy by means of separate pumping units (four single-passage pumps, each at 10 lb/sec).

For each application 18 configurations were considered initially. For the larger pumps the outer fluid radius $r_{3,4}$ was held at 2.0, 2.5, and 3.0 inches while the fluid velocity $\vec{v}_f$, was varied from 20 to 70 feet per second in steps of 10 feet per second. Since the mass flow rate was fixed at 40 pounds per second, the inner fluid radius $r_{2,3}$ could be calculated. For the quadruple-passage pump the thickness of the separators was assumed to have a negligible effect on flow rate.

The dimensions of the pumps having smaller capacities (10 lb/sec) were determined by choosing fluid velocity and fluid gaps ($g_f = r_{3,4} - r_{2,3}$) equal to those of each of the 18 corresponding larger pumps. In this way, the relative importance of hydraulic losses and electrical characteristics is about the same for both sizes, and more direct comparisons are possible.

By choosing appropriate values of excitation ampere-turns NI, working curves of efficiency η_s as a function of slip s for fixed developed pressure were generated for each fluid velocity and each pump configuration (fig. 5). Figure 5 shows efficiency η_s as a function of slip for an outer fluid radius $r_{3,4}$ of 2.0 inches and fluid velocities of 20 to 70 feet per second. The curves associated with a given pump capacity and number of passages were grouped in three sets, each set being associated with a value of $r_{3,4}$

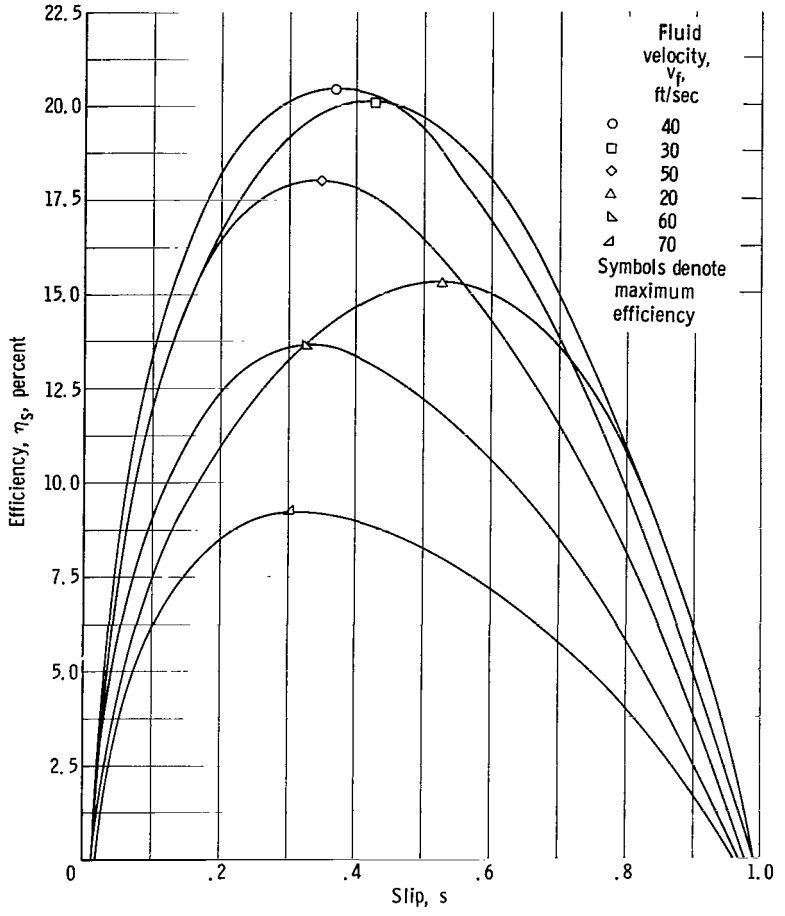

Figure 5. - Efficiency as function of slip for lithium pump at 1200° F. Number of passages, 1; fixed developed pressure, 30 pounds per square inch; flow, 40 pounds per second; outer fluid radius, 2.0 inches.

of 2.0, 2.5, or 3.0 inches. For each set, values of maximum efficiency η_v, over a slip range of 0 to 1, were obtained for each fluid velocity and plotted as a function of fluid velocity as is done in figure 6. From curves such as the one in figure 6, optimum fluid velocities, based on maximization of η_v, associated with each value of $r_{3,4}$ were obtained. From an analysis of these results it became clear that maximum efficiency could usually be attained by making the outer fluid radius as small as possible. Weight is also reduced by minimizing $r_{3,4}$; however, a lower limit in size is reached when the flux in the inner core reaches the saturation flux density of the magnetic material. Therefore, all designs for which the maximum flux density in the inner core $|\vec{B}|_m$ was greater than an acceptable level were rejected. Since the cores were assumed to be high-cobalt iron, this level was set at 14 000 gauss, this value being somewhat conservative as the saturation flux of high-cobalt irons at 1200° F is nearer 16 000 gauss. To obtain the final design, curves of $|\vec{B}|_m$ and efficiency as functions of $r_{3,4}$ at optimized fluid velocity were plotted and extrapolated to lower values of $r_{3,4}$ for which the

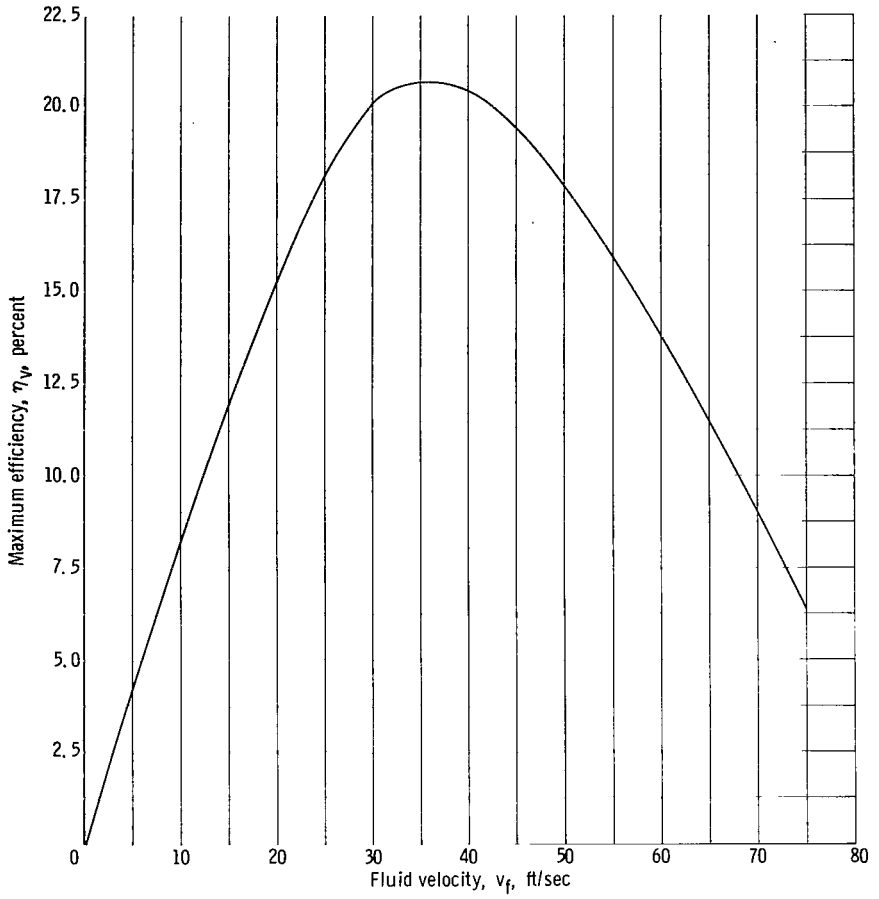

Figure 6. - Maximum efficiency as function of fluid velocity for lithium pump at 1200° F. Number of passages, 1; fixed developed pressure, 30 pounds per square inch; flow, 40 pounds per second; outer fluid radius, 2.0 inches.

maximum core flux density $|\vec{B}|_m$ was equal to 14 000 gauss. This $|\vec{B}|_m$ value was selected as the final choice unless a better efficiency was obtained at a lesser core flux density in a larger pump, in which case highest efficiency was the criterion for selection. By plotting optimized fluid velocity as a function of $r_{3,4}$, the final fluid velocity and therefore the final value of $r_{2,3}$ were determined.

Finally, an attempt was made to reduce the weight of the selected pumps by making the distance between coils x as small as possible and thereby reducing the required coil height h. The product hw is fixed since j_c is fixed, and NI is fixed by the requirement of 30 pounds per square inch of developed pressure. In all of the final pump selections, however, the flux density in the outer core was far from saturation, and the values of x that would produce such a condition were so small that a well-defined air gap might not exist, and thus the validity of the analysis would be questionable. It was decided, therefore, to limit the coil width w in each case to a value less than or equal to x whether or not $|\vec{B}|_m$ in the outer core was near saturation. As a result, all the

final pump selections are such that $x = w = 0.5$ inch.

RESULTS AND DISCUSSION

General Remarks

As mentioned earlier, an evaluation of the first set of computations made in the optimization procedure seemed to indicate that maximum efficiency and lowest weight could be attained by making the pump as small as possible without saturating the inner core (e.g., making the outer fluid radius $r_{3,4}$ small). The reason is that, for large fluid gaps and small wetted perimeters, hydraulic losses are low and thus fluid velocities can be made higher. At high fluid velocities the body forces exerted by the magnetic field, and therefore the pressure rise through the pump, can be made sizable without necessitating excessively high slip and low efficiency. High-flow pumps, therefore, tend to be more efficient than low-flow pumps; however, if $r_{3,4}$ is made large and the gap correspondingly small, hydraulic losses become more significant and high fluid velocities are not possible without degradation of efficiency. This occurs even though the required number of ampere-turns is less.

The criterion of minimum $r_{3,4}$ consistent with an unsaturated inner core was used for the selection of the pump having a weight flow of 10 pounds per second and a pressure rise of 30 pounds per square inch; however, it was noticed in optimizing the larger pumps that reducing $r_{3,4}$ below a certain value tended to decrease efficiency and increase weight. The peak at which maximum efficiency occurred was not sharp, but decreasing $r_{3,4}$ below this peak resulted in small, but consistent, decreases in efficiency and similar increases in weight. Two of the several reasons for such behavior are the following. First, even though hydraulic losses decrease with $r_{3,4}$, the required number of ampere-turns per coil increases because of the larger gap, and the losses in the coils are thereby increased and, for constant current density j_c, the coil height and the pump weight are increased.

Second, as the magnetic gap becomes large, the axial component of the magnetic field becomes large and the radial component becomes correspondingly small. The situation is depicted in figure 7 for zero slip and zero duct wall thickness. The zero-slip case was selected because the magnetic field is dependent on geometry alone, and the effect of large gaps on the magnetic-field shape and strength can be illustrated more clearly. In this case magnetic flux lines exit and reenter the outer core at points equidistant from a point of peak surface current density $\vec{S}$. The flux lines exiting and entering at points in the vicinity of zero $\vec{S}$ are more likely to include the inner core as part of their path than are flux lines that exit and enter the outer core nearer points of peak $\vec{S}$.

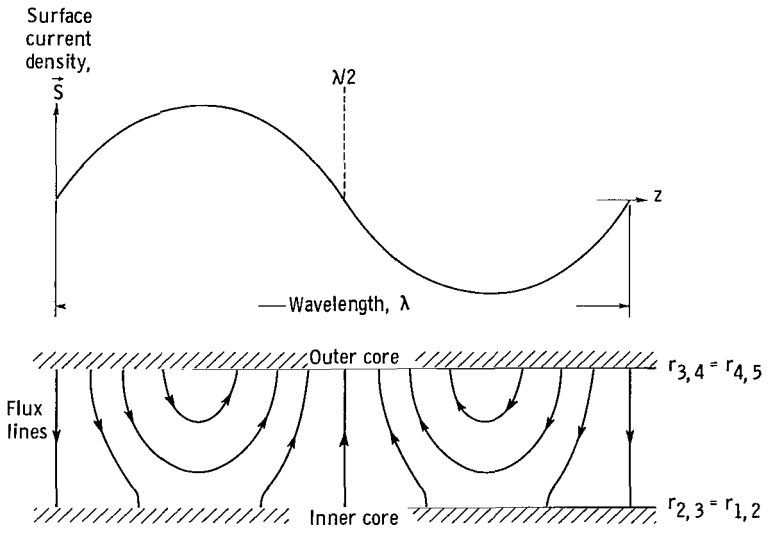

Figure 7. - Distribution of magnetic field across duct for zero slip and zero duct wall thickness.

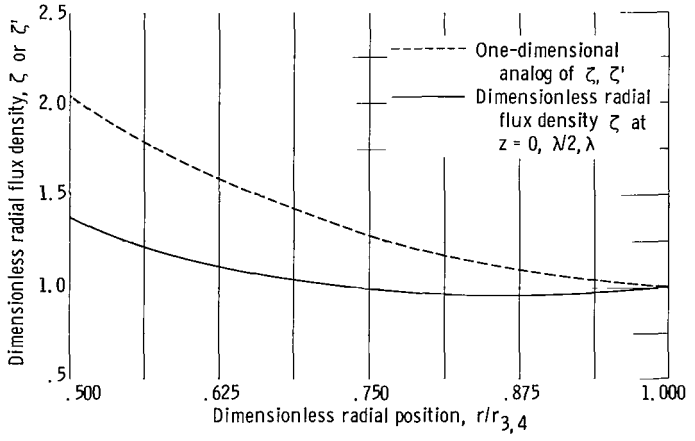

Figure 8. - Variation of magnetic-field strength across duct for zero slip and zero duct wall thickness.

The former have primarily a radial component of flux; whereas, the latter have primarily an axial component of flux except near the outer core. Furthermore, as the gap is increased, the flux lines not penetrating the inner core become comparatively more dense than those which do. The result is that, except near the outer core, the radial component of flux decreases with increasing gap and, therefore, so does the pumping force. Additional ampere-turns and, as a result, larger coil electrical losses are needed to compensate for this effect.

It is noteworthy that an analysis which allows the existence of both radial and axial components of magnetic-field strength is necessary in order to be able to analyze pumps with relatively large gaps. To show that two-dimensional effects are not necessarily negligible, a plot of dimensionless radial magnetic-field strength $\zeta = B_r(r)/B_r(r_{3,4})$ is given in figure 8 for the final configuration of the 40-pound-per-second single-passage pump. The zero-slip case is again chosen for purposes of illustration, and the plot is made for the fixed axial location $z = 0$ (see fig. 7) and various radial locations between the inner and outer core.

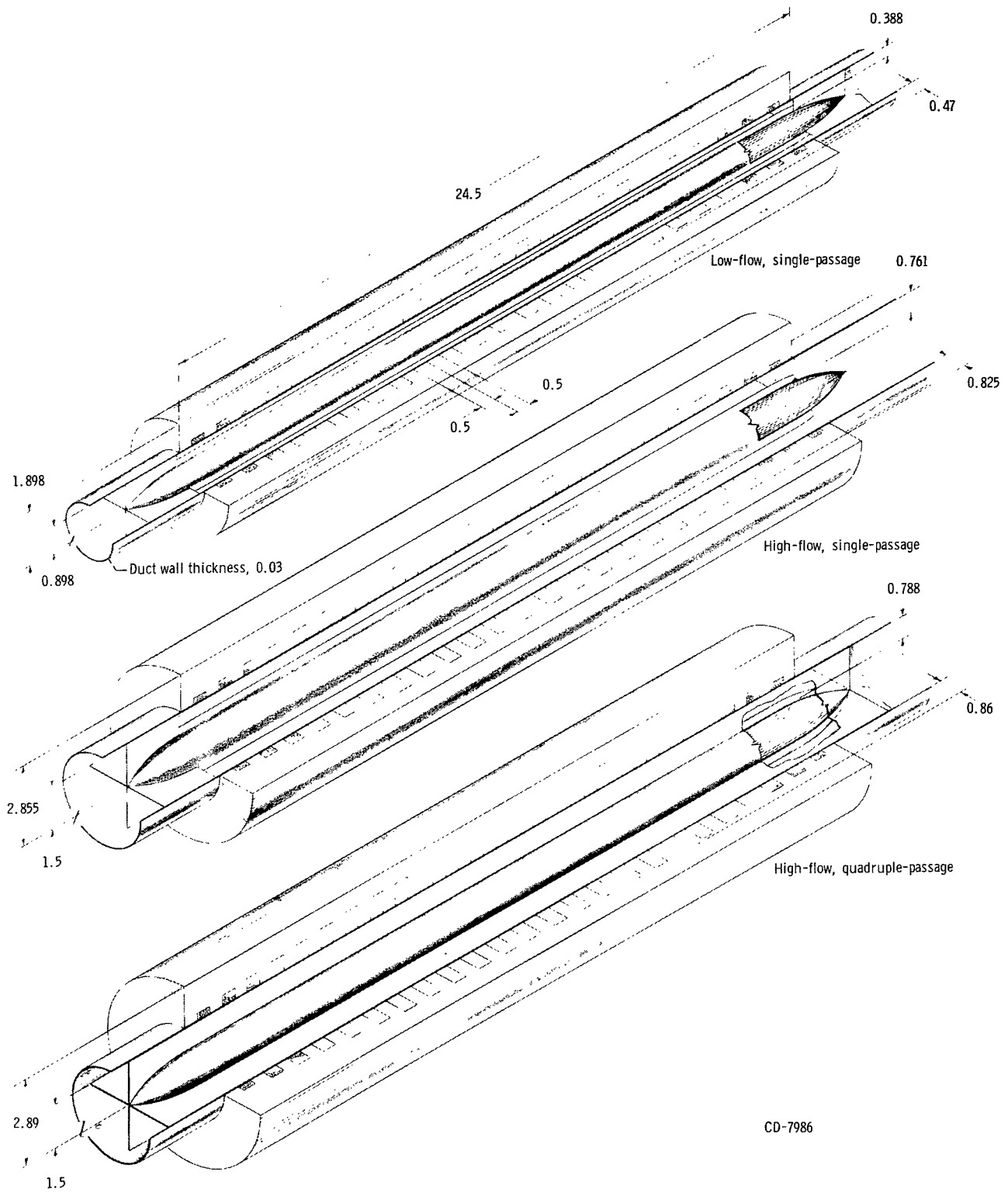

Figure 9. - Final pump configurations. (All dimensions in inches.)

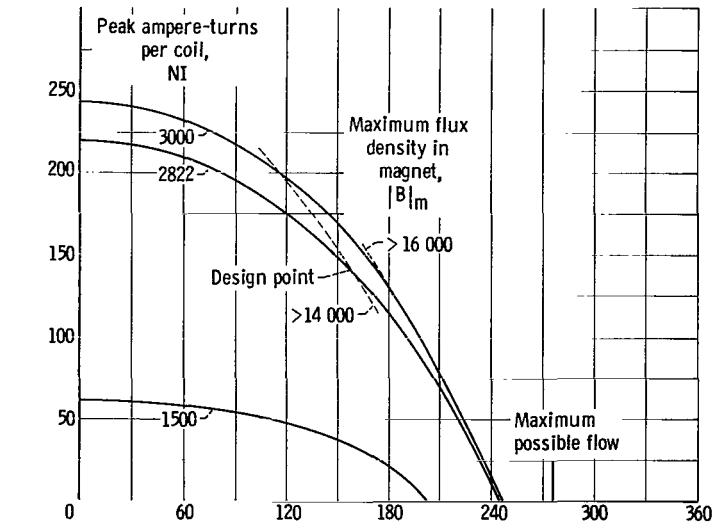

(a) Single-passage pump; flow rate, 10 pounds per second.

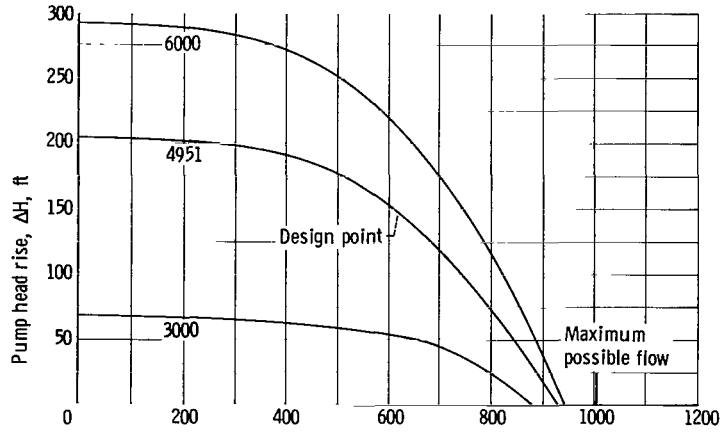

(b) Single-passage pump; flow rate, 40 pounds per second.

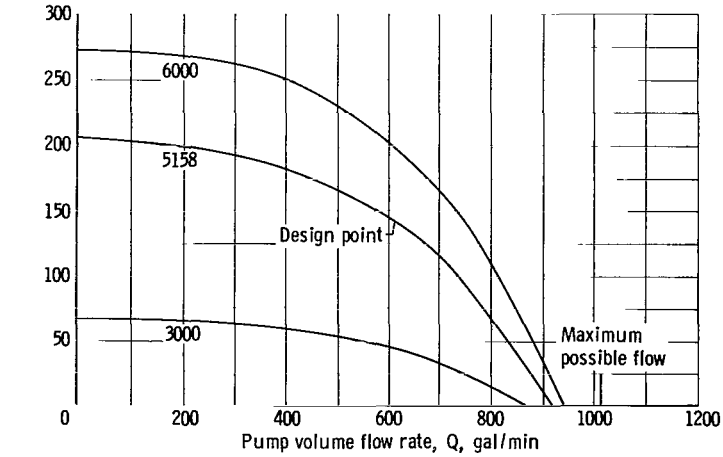

(c) Quadruple-passage pump; flow rate, 40 pounds per second.

Figure 10. - Pump head rise as function of flow rate for optimum lithium radiator coolant pumps. Developed pressure, 30 pounds per square inch.

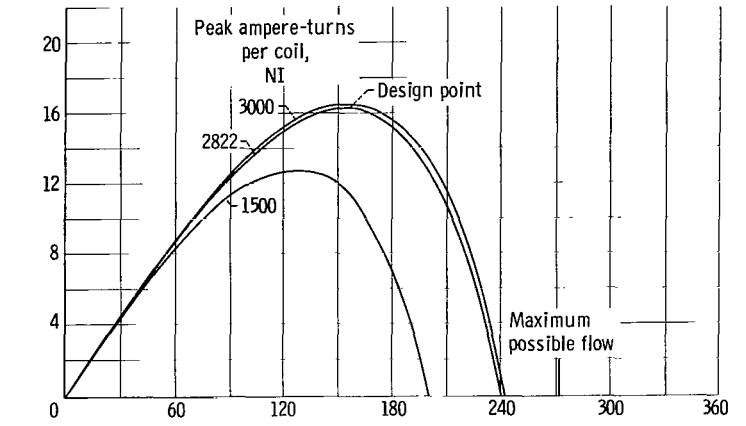

(a) Single-passage pump; flow rate, 10 pounds per second.

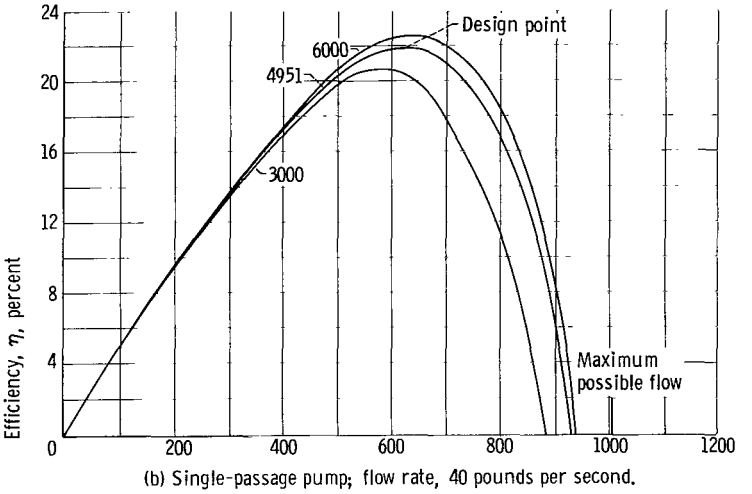

(b) Single-passage pump; flow rate, 40 pounds per second.

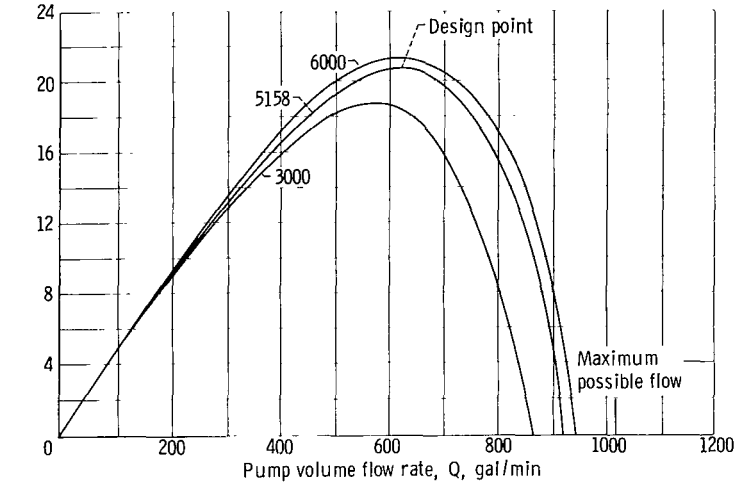

(c) Quadruple-passage pump; flow rate, 40 pounds per second.

Figure 11. - Efficiency as function of flow rate for optimum lithium radiator coolant pumps. Developed pressure, 30 pounds per square inch.

TABLE I. - DESIGN CHARACTERISTICS OF SELECTED PUMPS

Characteristic	Pump		
	Low-flow, single-passage (four units)	High-flow, single-passage (one unit)	High-flow, quadruple-passage (one unit)
Mass flow rate, lb/sec	10	40	40
Pump volume flow rate, gal/min	154	616	616
Frequency of exciting currents, cps	103	121	120
Velocity, ft/sec	28.8	37.0	36.1
Slip	0.44	0.39	0.40
Total pump output power, kW	2.01	8.04	8.04
Pump efficiency, percent	16.4	21.9	20.7
Total weight, lb	68(4) = 272	145	149
Weight-power ratio or specific weight of pump	33.7	18.0	18.5
Power factor	0.79	0.77	0.79
Maximum radius, $r'_{5,6}$, in.	1.898	2.855	2.890
Radius, $r_{3,4}$, in.	0.898	1.500	1.500
Magnet gap height, $r_{4,5} - r_{1,2}$, in.	0.388	0.761	0.788
Coil height, in.	0.470	0.825	0.860
Peak ampere-turns per coil	2822	4951	5158
Maximum flux density in magnet, G	14 000	9637	10 120
Required net positive suction head, ft	12.9	21.2	20.3

This plot is to be compared with the plot of the dimensionless magnetic field $\zeta' = r_{3,4}/r$, which is the counterpart of ζ for the case where, for analytical convenience, only a radial component of flux is assumed to exist. Such a one-dimensional assumption leads to the requirement that the radial component of flux, which is the only component, must vary inversely with radius in order to conserve flux. It is to be noted that the dimensionless parameter ζ, at $z = 0$, differs appreciably from the dimensionless parameter ζ'. A two-dimensional analysis, such as the one outlined in the present report, is therefore desirable.

Final Pump Configurations

Final pump configurations are depicted in figure 9. Curves showing head and efficiency as functions of flow for each of the pumps selected are presented in figures 10 and 11. The design characteristics for each pump are listed in table I for the following conditions:

Fluid . . . . . Lithium
Pump pressure rise, Δp, lb/sq in. 30

Pump head rise, ΔH, ft	147.44
Temperature, ^{o}F	1200
Length, in.	24.5
Wavelength, λ, in.	6
Number of wavelengths, d	4
Duct	Columbium - 1 percent zirconium
Duct wall thickness, τ, in.	0.03
Coil	Copper at 1200^{o} F
Coil width, w, in.	0.5
Peak coil current density, j_c, A/sq in.	12 000
Magnetic material	High-cobalt iron at 1200^{o} F

In figures 10 and 11 the performance of each pump for two values of excitation ampere-turns other than the design value is given. For the larger pumps considered the peak efficiency was reached at an $r_{3,4}$ of approximately 1.5 inches. Since deviations from this value of $r_{3,4}$ produced changes in efficiency of only about 0.5 percent per inch, further trials were deemed unnecessary. The optimum fluid velocity for the quadruple-passage 40-pound-per-second pump was slightly less than that for the single-passage 40-pound-per-second pump, and, hence, the radius of the inner core was necessarily somewhat smaller for the former.

For large values of NI and low flow rates, where hydraulic losses are not as significant as electrical losses, head increases linearly with I^2 for a given flow and number of turns N. Electrical losses also vary as I^2 for this case. As a result, the curves of efficiency as a function of flow approach each other as NI is increased, efficiency being relatively unaffected by hydraulic losses and dependent primarily on geometry, which is fixed.

For each pump, a line indicating the maximum possible flow is given; this line represents that flow for which fluid and wave velocities are equal. In figure 10(a), curves of constant maximum core flux density are also plotted for $|\vec{B}|_m$ = 14 000 and 16 000 gauss. Between these two curves the validity of the performance curves given should be considered borderline; to the right of the 16 000 gauss line the performance curves should be used with caution. Performance past this point is possible, however, since $|\vec{B}|_m$ is only a peak value. No constant maximum core flux density curves are plotted for the higher flow pumps since they should be in no danger of saturation.

Table II presents weight and efficiency comparisons for pumps with different coil current density and duct materials but with the same head, flow, internal dimensions, wavelength, and frequency. Coil current density is somewhat arbitrary, efficiency and weight both increasing with decreasing j_c. Duct material is also somewhat arbitrary, although it is felt that, on the basis of current information, columbium - 1 percent

TABLE II. - EFFECT OF DUCT MATERIAL AND COIL CURRENT DENSITY ON PERFORMANCE CHARACTERISTICS FOR LITHIUM RADIATOR COOLANT PUMPS

[Pump pressure rise, 30 lb/sq in.]

Peak coil current density, A/sq in.	Duct wall material	Peak ampere-turns per coil, NI	Weight, lb	Weight-power ratio or specific weight of pump, lb/kW	Efficiency, percent
10-lb/sec pump; total pump output, 2.01 kW; number of passages, 1					
[a]12 000	Columbium 1 percent zirconium	2822	68	33.7	16.4
12 000	Tantalum alloy (T-111)	2786	69	34.4	16.8
12 000	Infinite resistor	2632	67	33.3	19.5
6 000	Columbium - 1 percent zirconium	2822	113	56.1	22.4
0	Columbium - 1 percent zirconium	2822	∞	∞	35.2
0	Infinite resistor	2632	∞	∞	48.2
40-lb/sec pump; total pump output, 8.04 kW; number of passages, 1					
[a]12 000	Columbium - 1 percent zirconium	4951	145	18.0	21.9
12 000	Tantalum alloy (T-111)	4892	146	18.2	22.2
12 000	Infinite resistor	4712	143	17.7	24.7
6 000	Columbium - 1 percent zirconium	4951	271	33.7	29.3
0	Columbium - 1 percent zirconium	4951	∞	∞	44.5
0	Infinite resistor	4712	∞	∞	55.0
40-lb/sec pump; total pump output, 8.04 kW; number of passages, 4					
[a]12 000	Columbium - 1 percent zirconium	5158	149	18.5	20.7
12 000	Tantalum alloy (T-111)	5123	151	18.7	21.1
12 000	Infinite resistor	4934	147	18.2	23.3
6 000	Columbium - 1 percent zirconium	5158	277	34.5	27.7
0	Columbium - 1 percent zirconium	5158	∞	∞	42.1
0	Infinite resistor	4934	∞	∞	51.6

[a]This row represents selected pump design.

zirconium is the most probable material for use with lithium. A tantalum alloy (T-111) is also a possible material and the only refractory metal being considered for space applications with a higher resistivity than columbium - 1 percent zirconium. As can be seen, there is only a slight improvement in efficiency for the T-111 duct with a slight increase rather than a decrease in weight. This corresponds to the fact that tantalum is only slightly more resistive than columbium but weighs approximately twice as much.

Decreasing coil current density appears to be a good means of increasing efficiency. Unfortunately, sizable increases in weight due to increased coil height result from low current densities. If efficiency were the primary criterion for selection, a much lower current density than that assumed for the chosen design (peak value, 12 000 A/sq in.) would be appropriate. It would also be advantageous to cool the coils as much as possible to keep coil resistivity down; however, in this case it was felt that low weight was the primary criterion, and therefore j_c = 12 000 amperes per square inch was assumed. This value is probably as high a current density as is practical in ordinary conductors such as copper. For such a high current density a good thermal conduction path from coil to coolant is necessary in order to minimize increases in coil electrical resistivity with temperature.

With the assumed peak value of coil current density of 12 000 amperes per square inch, the efficiencies obtained for the 10-pound-per-second single-passage, 40-pound-per-second single-passage, and 40-pound-per-second quadruple-passage pumps were, respectively, 16.4, 21.9, and 20.7 percent. The total weights were 272 (four pumps, each weighing 68 lb), 145, and 149 pounds.

In comparison, references 1 to 3 give an efficiency of 15 percent and a weight of 85 pounds for an annular traveling-wave pump operating with a pressure rise of 20 pounds per square inch and a flow rate of 8 pounds per second. The application here is also as a radiator coolant pump for lithium.

The efficiencies and weights of the pump designs obtained in this report are, therefore, reasonable for use in space power systems and compare favorably with other traveling-wave pump designs. Furthermore, the values of weight and efficiency for the high-flow quadruple-passage pump as compared with the weight and efficiency of four low-flow single-passage pumps indicate that the use of multiple passages in a single pumping unit may be a desirable pumping method in parallel-loop systems.

SUMMARY OF RESULTS

An analysis of the annular traveling-wave pump has been made that accounts for the two-dimensional distribution of magnetic field and for effects of pump geometry and duct and fluid conductivity on the magnetic field. This method was applied to the design of

several lithium radiator coolant pumps suitable for application in a space powerplant, and the following results were obtained:

1. Designing for the highest fluid velocity attainable without incurring excessive hydraulic losses appears to be a practical objective since high fluid velocity allows high output pressure without necessitating high slip.

2. In general, relatively higher fluid velocities, larger gaps, and smaller fluid radii than those used in the past lead to best efficiencies and weights.

3. Better efficiencies and weights are obtainable for high-flow pumps than for low-flow pumps.

4. A simple but effective means of attaining higher pump efficiencies is to decrease the coil current density. If this is to be done, however, it must be at the expense of increased pump weight.

5. The use of a single unit with multiple passages rather than separate pumping units for redundancy allows higher efficiencies and lower weights than could be obtained otherwise. The performance of such a pump could seriously deteriorate, however, by the loss of fluid in one or more of its passages due to the increased current path length. Behavior of such pumps under conditions involving the loss of fluid in one or more passages has not been evaluated.

6. For the particular pumps considered, a tantalum duct wall has no significant advantages in terms of efficiency and weight over a columbium - 1-percent-zirconium duct wall.

7. Efficiencies and weights were obtained for several lithium radiator coolant pumps for a design pressure rise of 30 pounds per square inch. A single-passage 10-pound-per-second pump with an efficiency of 16.4 percent and a total system weight of 272 pounds (four pumps, each weighing 68 lb) was designed. Designs were also obtained for single- and quadruple-passage 40-pound-per-second pumps with efficiencies of 21.9 and 20.7 percent and weights of 145 and 149 pounds, respectively. These values of efficiency and weight compare favorably with other pumps designed for application in space power systems.

Lewis Research Center,
National Aeronautics and Space Administration,
Cleveland, Ohio, January 13, 1965.

APPENDIX - SYMBOLS

A_f	fluid cross-sectional area
a_1	coefficient of Bessel function J_1
a_2	coefficient of Bessel function Y_1
$\vec{B}$	magnetic-field strength or flux density
$\lvert\vec{B}\rvert_m$	maximum flux density in magnet
B_r	radial component of magnetic-field strength or flux density
B_z	axial component of magnetic-field strength or flux density
b_1	coefficient of Bessel function J_0
b_2	coefficient of Bessel function Y_0
C_f	friction factor
d	number of wavelengths in pump
$\vec{E}$	electric field intensity
g_f	fluid gap height, $r_{3,4} - r_{2,3}$
g_m	magnet gap height, $r_{4,5} - r_{1,2}$
ΔH	pump head rise
h	coil height
I	peak current per coil
J_0, J_1	Bessel functions of the first kind
$\vec{j}$	electrical current density
j_c	coil electrical current density
k	wave number of magnetic wave, $2\pi/\lambda$
ΔM_λ	increase in pump weight per wavelength due to nonzero coil height
m	integer denoting relation to mth component of magnetic field
N	number of turns per coil
NI	peak ampere-turns per coil
$\hat{n}$	unit vector normal to interface between mediums G and H
Δp	pump pressure rise
Δp_λ	pressure rise per wavelength due to magnetic-electric forces
$\Delta p_{n\lambda}$	net pressure rise per wavelength, $p_\lambda - \Delta p_{V\lambda}$
$\Delta p_{V\lambda}$	pressure drop per wavelength due to viscous forces
Q	pump volume flow rate
q	number of passages
R	coil resistance
$\vec{R}$	vector function containing entire dependence of $\vec{B}$ on r
Re	Reynolds number
r	radial coordinate
S	peak value of $\vec{S}$
$\vec{S}$	surface current density
s	slip
t	time
$\vec{v}$	velocity of any medium
$\vec{v}_f$	fluid velocity
v_s	slip velocity
$\vec{v}_w$	magnetic wave velocity
W_λ	output power per wavelength due to magnetic-electric forces
$W_{c\lambda}$	Ohmic heat loss per wavelength in coils

$W_{J\lambda}$	Ohmic heat loss per wavelength, sum of fluid duct and core losses
$W_{J\lambda,\ell}$	Ohmic heat loss per wavelength in medium ℓ
$W_{n\lambda}$	net pump output power per wavelength, $W_\lambda - W_{V\lambda}$
$W_{T\lambda}$	total pump input power per wavelength
$W_{V\lambda}$	power loss per wavelength due to viscous forces
w	coil width
w_{sp}	weight-power ratio or specific weight of pump
x	distance between coils
Y_0, Y_1	Bessel functions of second kind
z	axial coordinate
α	component of $\vec{R}$ in r-direction
β	component of $\vec{R}$ in z-direction
γ	complex number defined in eq. (11)
$\delta_{x,y}$	1 if $x = y$, 0 if $x \neq y$
ζ	dimensionless radial magnetic-field strength or flux density
ζ'	one-dimensional analog of ζ
η	pump efficiency
η_s	intermediate values of η obtained by assuming head, flow, fluid velocity, and outer fluid radius fixed and slip varying
η_v	intermediate values of η obtained by maximizing η_s over full range of slip for each fluid velocity assumed
θ	circumferential coordinate
λ	wavelength of traveling wave
μ	magnetic permeability
μ_f	fluid absolute viscosity
ρ_c	density of coil
ρ_f	fluid density
ρ_m	density of magnetic material
σ	electrical conductivity
τ	duct wall thickness
Φ	phase angle
ω	frequency of exciting currents

Subscripts:

c	coil
G	medium G
G, H	interface between mediums G and H
H	medium H
id	ideal
ℓ	medium ℓ
$\ell+1$	medium $\ell + 1$
$\ell, \ell+1$	interface between mediums ℓ and $\ell + 1$

Superscripts:

$(\vec{\ })$	vector
$(\hat{\ })$	unit vector
$(')$	real as opposed to ideal pump dimensions

REFERENCES

1. Verkamp, J. P.: Electromagnetic Alkali Metal Pump Research Program. Quarterly Prog. Rept. No. 1, General Electric Co., Nov. 8, 1963.

2. Verkamp, J. P.: Electromagnetic Alkali Metal Pump Research Program. Quarterly Prog. Rept. No. 2, General Electric Co., Feb. 17, 1964.

3. Verkamp, J. P.: Electromagnetic Alkali Metal Pump Research Program. Quarterly Prog. Rept. No. 3, General Electric Co., May 22, 1964.

4. Einstein, A.; and Szilard, L.: Electrodynamic Movement of Fluid Metals Particularly for Refrigerating Machines. Patent Specification No. 303, 065 (Germany), Dec. 27, 1927; No. 38, 091/28 (United Kingdom), May 26, 1930.

5. Okhremenko, N. M.: Electromagnetic Phenomena in Flat-Type Induction Pumps for Molten Metal. ARS J. (Russian Supp.), vol. 32, no. 9, Sept. 1962, pp. 1442-1448.

6. Turcotte, D. L.; and Lyons, J. M.: A Periodic Boundary-Layer Flow in Magnetohydrodynamics. J. Fluid Mech., vol. 13, pt. 4, Aug. 1962, pp. 519-528.

7. Hartmann, J.: Mercury Dynamics. I - Theory of the Laminar Flow of an Electrically Conductive Liquid in a Homogeneous Magnetic Field. Kgl. Danske Videnskab. Selskab. Math.-fys. Medd., vol. 15, no. 6, 1937.

8. Murgatroyd, W.: Experiments on Magnetohydrodynamic Channel Flow. Phil. Mag., ser. 7, vol. 44, no. 359, Dec. 1953, pp. 1348-1354.

9. Vennard, J. K.: Elementary Fluid Mechanics. John Wiley & Sons, Inc., 1947, pp. 157-161.

2/22/85

"The aeronautical and space activities of the United States shall be conducted so as to contribute . . . to the expansion of human knowledge of phenomena in the atmosphere and space. The Administration shall provide for the widest practicable and appropriate dissemination of information concerning its activities and the results thereof."

—NATIONAL AERONAUTICS AND SPACE ACT OF 1958

NASA SCIENTIFIC AND TECHNICAL PUBLICATIONS

TECHNICAL REPORTS: Scientific and technical information considered important, complete, and a lasting contribution to existing knowledge.

TECHNICAL NOTES: Information less broad in scope but nevertheless of importance as a contribution to existing knowledge.

TECHNICAL MEMORANDUMS: Information receiving limited distribution because of preliminary data, security classification, or other reasons.

CONTRACTOR REPORTS: Technical information generated in connection with a NASA contract or grant and released under NASA auspices.

TECHNICAL TRANSLATIONS: Information published in a foreign language considered to merit NASA distribution in English.

TECHNICAL REPRINTS: Information derived from NASA activities and initially published in the form of journal articles.

SPECIAL PUBLICATIONS: Information derived from or of value to NASA activities but not necessarily reporting the results of individual NASA-programmed scientific efforts. Publications include conference proceedings, monographs, data compilations, handbooks, sourcebooks, and special bibliographies.

Details on the availability of these publications may be obtained from:

SCIENTIFIC AND TECHNICAL INFORMATION DIVISION

NATIONAL AERONAUTICS AND SPACE ADMINISTRATION

Washington, D.C. 20546